Development of a Ballistic Impact Detection System

Stephen A. Van Albert and Paul F. Bruney III
Walter Reed Army Institute of Research
Division of Military Casualty Research
Silver Spring, Maryland 20910

Steve.VanAlbert@NA.Amedd.Army.Mil

ABSTRACT

The Future Force Warrior program is a revolutionary redesign of the warfighter platform that, for the first time, will incorporate soldier-worn physiological monitoring equipment. Part of this physiological system will include a Ballistic Impact Detection System (BIDS), designed to detect potentially injurious impacts to the body. Proof-of-concept data showed a consistent biphasic vibration pattern consisting of low amplitude, high frequency (Avg 656.6, SD 96.3 Hz) segment followed by a higher amplitude low frequency (98 Hz) segment. Low velocity impacts have shown that similar vibration patterns are created in the live swine (490.4 Hz, SD 118.1 Hz), dead swine (Avg 494.9 Hz, SD 123.0 Hz) and live human (Avg 437.1 Hz, SD 78.6 Hz). High velocity impact experiments in swine have been the basis for the design of an analogue/digital circuit that discriminates between normal activity and bullet and blast overpressure and fragment surrogates.

1.0 INTRODUCTION

The future battlefield is projected to be asymmetric, non-contiguous and nonlinear. To meet the challenge of future conflicts, the U.S. Army is changing its paradigm from linear and sequential operations to simultaneous and distributed operations. Sophisticated and adaptive adversaries are making unconventional tactics, such as guerrilla warfare and terrorist attacks, commonplace. In the future as today ground forces will continue to be counted on to win and hold the ground and rebuild the peace. The centrepiece enabler of the Army's transformation is the Future Force Warrior (FFW). FFW is a revolutionary redesign of the individual warfighter platform from the skin out. FFW is a system of systems – data from sensors on the individual soldier are fused with similar information from other soldiers in the unit of action. As the data is integrated and sent back, the warfighter becomes a sensor node in a bigger network mesh that ultimately allows battlefield commanders to quickly react to critical information. Elements of the individual warfighters health status will be incorporated into the data stream from physiological monitoring devices worn by each soldier. The Warfighter Personal Status Monitor (WPSM) is the overarching medical system that will deliver pertinent information that will keep the soldier in the fight and in the event of becoming a combat casualty, aid the medic in rescue and recovery operations.

The central tenet to the Army's transformation to FFW is the ability to "see first, understand first, act first and finish decisively [1]." The underlying foundation for achieving this detect-decide-deliver goal of battlefield tactics will be information technology. Acquiring critical information and delivering it rapidly and correctly will have a profound impact on the tactical, operational and strategic success of future combat missions. In the future, the Army unit of action will conduct operations over larger spaces. This translates into small, disparate fighting groups covering far more territory with a single medic in support. It is quite likely that FFW

Paper presented at the RTO HFM Symposium on "Combat Casualty Care in Ground Based Tactical Situations: Trauma Technology and Emergency Medical Procedures", held in St. Pete Beach, USA, 16-18 August 2004, and published in RTO-MP-HFM-109.

warfighters will be out of sight and hailing distance of medics and will rely on a medical information sub-network to achieve adequate levels of medical support. Early notification of a soldier's need for medical attention can reduce the time to initial treatment and thus may reduce the morbidity and mortality of wounded soldiers. The overall goal of the Ballistic Impact Detection System (BIDS) and WPSM program is to increase survivability of the soldier on the battlefield, and facilitate more rapid triage for the combat medic.

Data from Bellamy's study of causes of death from the Vietnam War [2] shows that while 66% of combat casualties die within the first 5 minutes of being wounded there is an opportunity to save lives if a medic can get to a soldier quickly. Figure 1 shows the percentage of all combat deaths as a function of the time from the wounding event. A therapeutic window of opportunity exists for those soldiers killed in action (KIA) in the timeframes encompassing 5 minutes to 6 hours. Given Carey's findings [3] during Operation Desert Storm that the predominant cause of deaths in Corps hospitals was exsanguination from extremity wounds, it is likely that with advances in body armour, extremity wounds will become a large percentage of potentially salvageable casualties on the battlefield. Knowing when a wounding event occurs and the ability to engage other physiological apparatus on the soldier to determine the extent of the casualty can play an important role in the required remote triage capability needed to change battlefield casualty statistics.

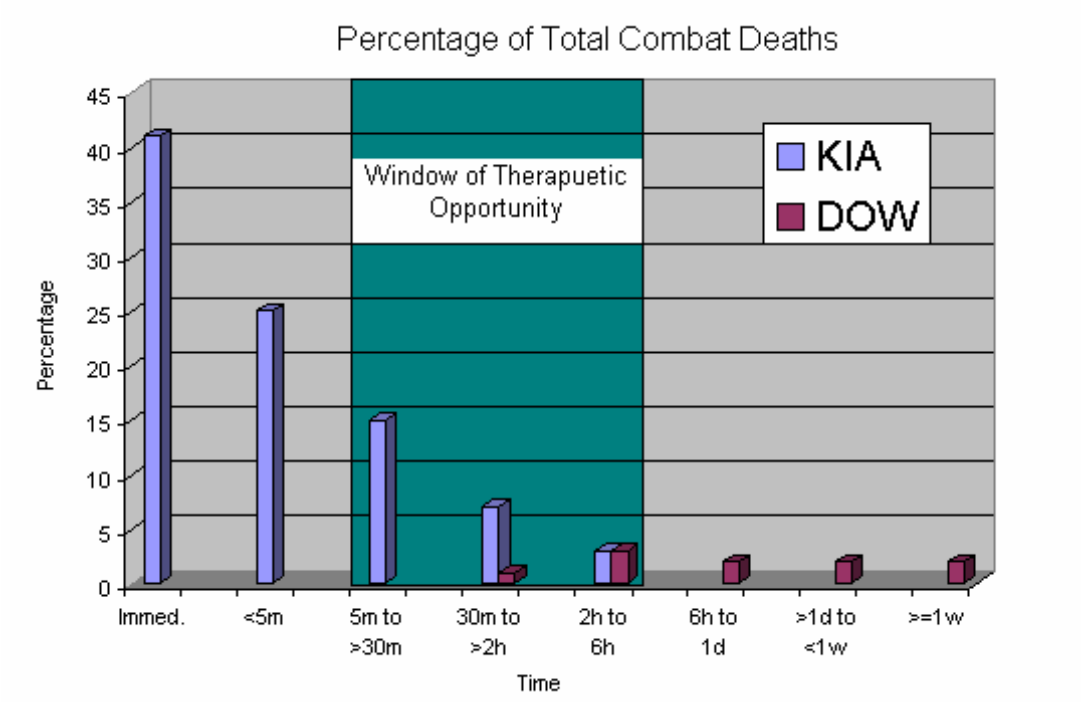

Figure 1

Source: Pearce, F.J. from Bellamy, R. F.

2.0 METHODS

The Ballistic Impact Detection System (BIDS) project began with the hypothesis that acoustic vibrations on the skin created by penetrating ballistic missiles could be sensed and analyzed to determine severity of the wounding event. A proof-of-concept phase was conducted with the acquisition of impact signatures from a swine model used in a non-lethal wounding protocol. During this protocol, a single 'plastic bullet' (a 12mm steel bearing ball with a thin plastic coating weighing approximately 16 g) was fired from a gas gun at an anesthetized pig from a distance of 8 feet. Three impact locations were used – lateral chest, sternum, and abdomen. Velocities ranged from 239 to 298 feet/second. Two piezo-film sensor elements were attached using duct tape to the back of the animal, symmetrically about the spine just below the scapulas or symmetrically about the sternum. The voltage response from the sensor elements were digitized at 20,000 samples per second and digitally recorded. Figure 2 shows an impact to the left lateral chest. This image was captured from a high-speed (4500 frames/sec) video recording for animal 65-4.

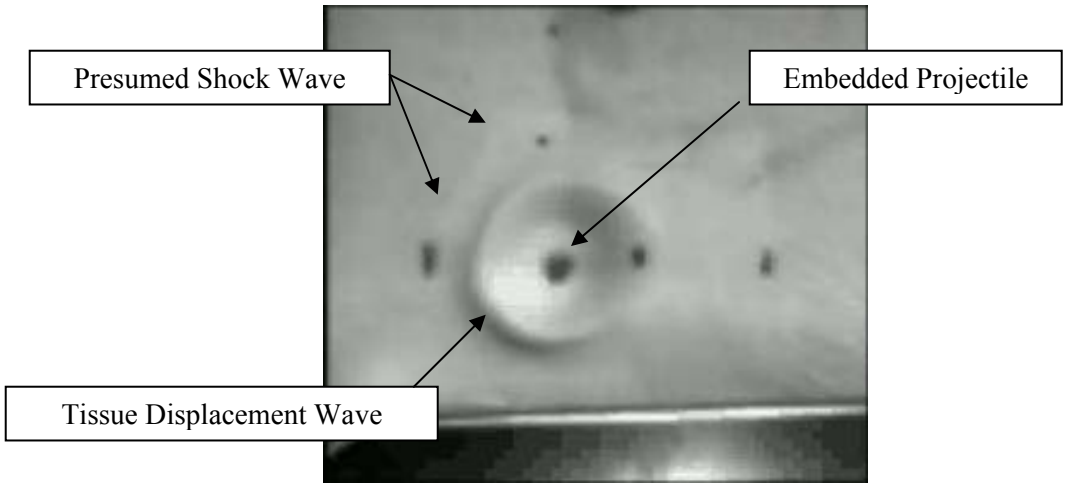

Figure 2

Analysis of the impact signatures showed consistent characteristics. Each waveform was made up of two distinct frequency patterns. The first pattern was a low-amplitude, high-frequency section lasting on the order of 20 ms. The second pattern was a high-amplitude low-frequency section. Figure 3 shows the voltage recording for ID 65-4.

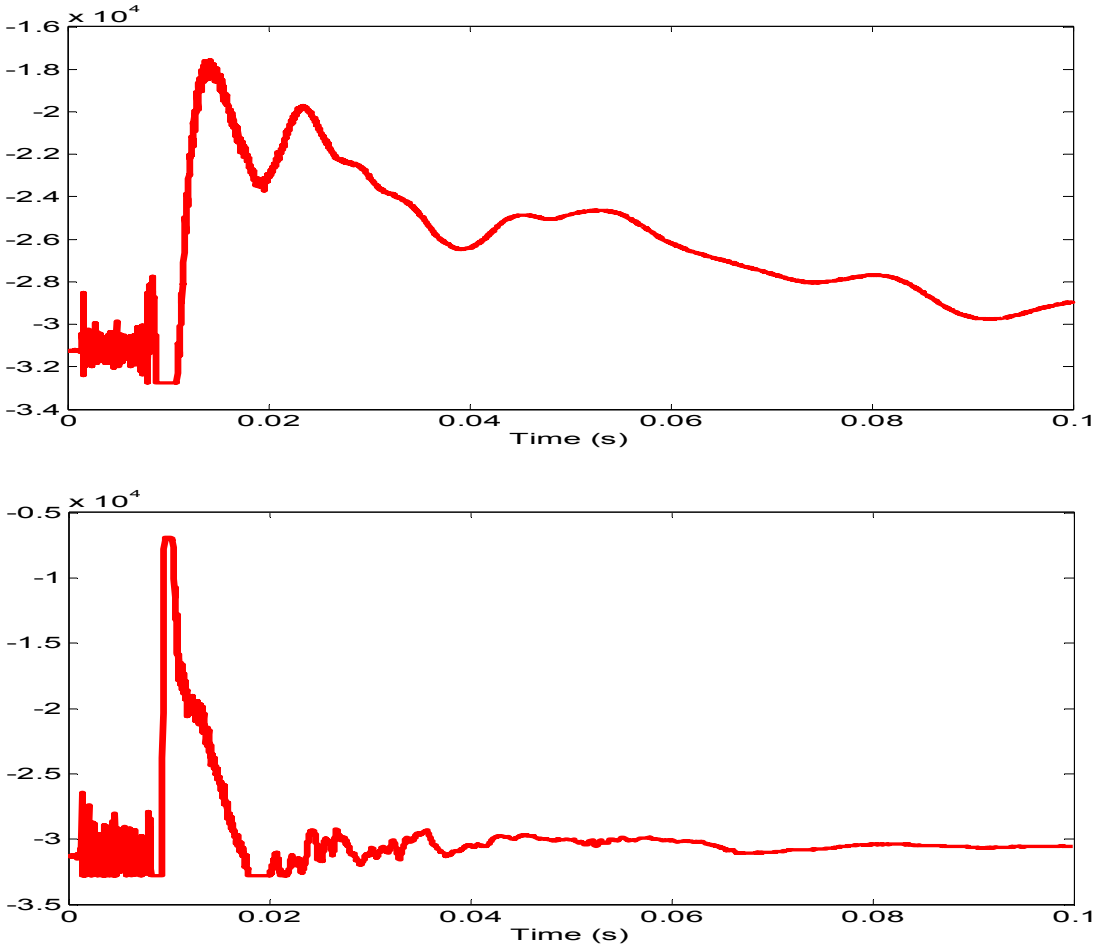

Figure 3

For our purposes, we will refer to the high frequency section as the shock wave and the lower frequency section as the tissue displacement wave. High-speed photography (Figure 2) shows the two frequency sections - the shock wave as a fast moving slight rippling effect that moves outward from the impact site and the slower developing tissue displacement wave radiating outward tantamount to ripples in a pool. Examination of Figure 3 shows that the shock wave amplitude of the left sensor is greater than the amplitude of the right sensor, confirming that the impact site was the left lateral chest. Examination of the tissue displacement waves also confirms a left side hit. They also show that once formed, they move rapidly as witnessed by the imperceptible delay of the tissue displacement waves between the sensors. Frequency analysis in the form of Fast Fourier Transforms (FFT) was performed on the waveforms. Figure 4 shows the FFT performed on the initial 7.5 ms of the shock wave for ID 65-4. Peak frequencies in the range from 500 to 1000 Hz were typical in all shots. The peak frequencies (frequencies with the highest power) in this range from this type on analysis are tabulated in Table 1. FFTs were also performed on the tissue displacement section of the waveform. In every case the predominant frequency of the tissue displacement wave was 98 Hz $\pm$ 19 Hz.

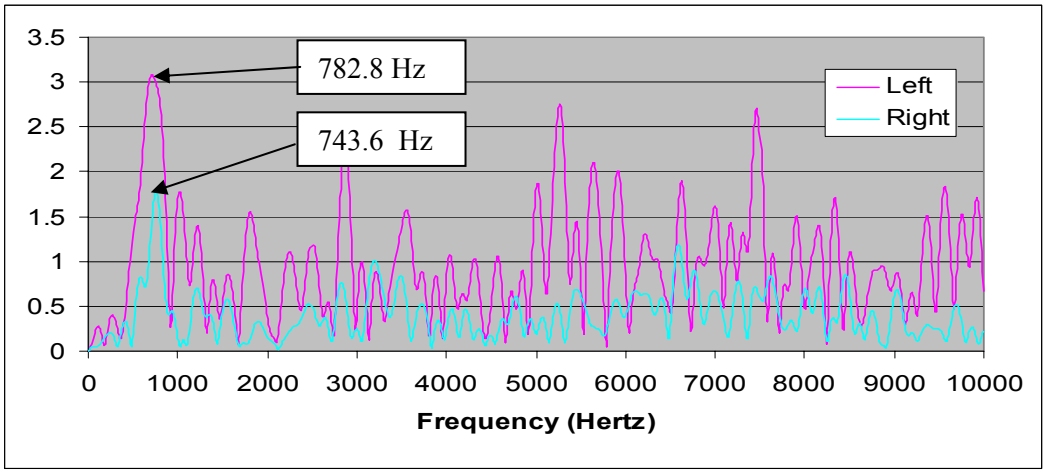

Figure 4

Animal ID	Primary Right Frequency	Primary Left Frequency	Impact Area
11-5	645.8	508.8	Stomach
12-11	763.2	547.9	Chest
12-9	665.4	743.6	Stomach
13-11	684.9	665.4	Chest
22-9	724.1	489.2	Abdomen
24-10	547.9	782.8	Chest
26-12	508.8	626.2	Sternum
65-1	606.6	645.8	Chest
65-2	821.9	645.8	Sternum
65-3	673.2	665.4	Chest
65-4	782.8	743.6	Chest
65-5	743.6	567.5	Abdomen
65-6	645.8	802.3	Abdomen
9-3	626.2	508.8	Chest
Average	674.30	638.79	
St Dev	88.07	104.01	

Table 1

The similarity of the primary frequencies provided a proof-of-concept for ballistic impact detection. The primary frequency range (489 – 822 Hz) of the impact signature is much higher than what is typically generated in the body during routine activity. Running, jumping and even blunt thumps to the body elicit only the typical 100 Hz tissue displacement frequency that was also seen in the ballistic signature analysis.

2.1 Low velocity impact models:

A multi-protocol research plan was developed to compare impact signatures across models with those from humans. For this purpose a commercial paintball rifle was chosen to deliver standardized impacts. Paintballs offered a socially acceptable method of delivering an impact to human volunteers for comparison to similar

swine and human cadaver impacts. Similarity of low velocity impact signatures with that of humans would build a strong case for the necessary high velocity impacts in that model.

Four swine weighing from 48 to 75 kg were impacted in four locations each (sternum, lateral chest, abdomen and hind leg) with and without body amour while under anaesthesia. Five paintballs were fired at each location for a total of forty shots per pig (4 locations x 5 shots with body amour plus 4 locations x 5 shots without body amour). Eight piezofilm sensors were attached to the pig's back in two columns of four, symmetrical about the spine. . The amour/non-amour portions of the testing were randomized, as was the shot order in each portion. However, all 20 shots were fired before changing into or out of the body amour. Similarly, all five shots per position were fired before changing to a different impact location. The animals were fitted with older versions of aviation flak jackets for these tests. A total of 1280 impacts recordings were acquired (4 pigs x 4 locations x 2 body amour x 5 shots x 8 sensors). Analysis revealed that while impacts were discernable for almost every sensor and every shot, many of the impact recordings were too low in amplitude and not similar to the non-lethal impacts seen in the proof-of-concept work. Load cell analyses of the paintball impacts show forces that are 25 times less than the solid steel balls used in the non-lethal phase. Calculated values for the non-lethal projectiles range from 46 to 66 Joules, at the velocities (250 – 300 ft/sec) used in the protocol. Paintball impacts can be calculated at 8 Joules (using 3 g and 250 ft/sec); however, this calculation does not consider the work expended as the paintball breaks upon impact. Paintball impacts were measured using a load cell at 2 Joules. It is suspected that the difference in the force of the impacts does not cause the characteristic impact signatures of the non-lethal wounding studies. A typical lateral chest with amour signature is shown in Figure 5.

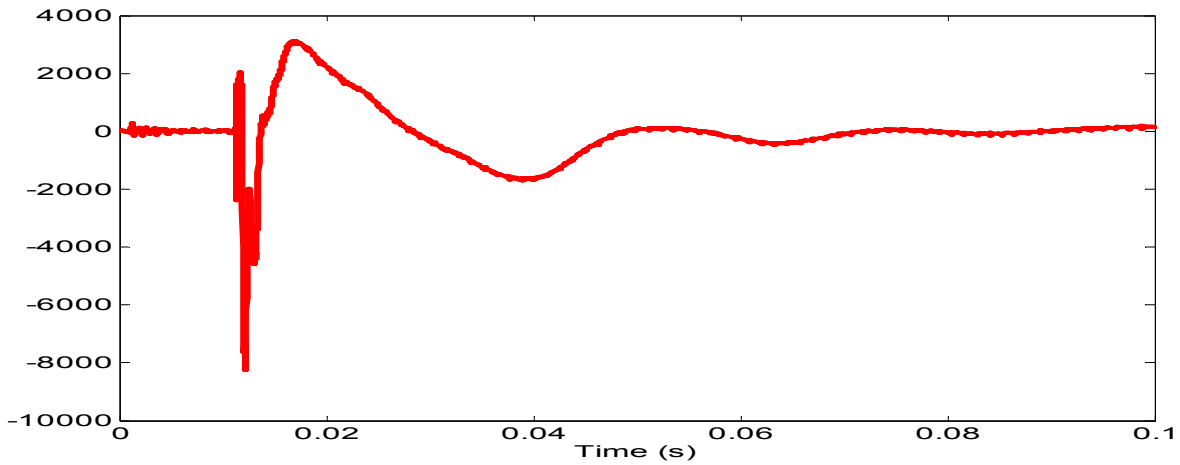

Figure 5

The signature in Figure 5 can be broken into three separate sections: the pre-impact section from 0 to 9 ms, the impact section from 9 to 12 ms and the tissue displacement section from 12 ms on. With no way of determining the actual time of impact of these recordings, we believe that the pre-impact section of the signatures represents the response from the air blast of the paintball rifle when fired. The impact section corresponds to the shock wave section in the non-lethal wounding signatures. Due to the diminished force of impact of the paintball, the impact section duration is shorter than the non-lethal signatures. The diminished force of impact also causes the amplitudes of the tissue displacement wave to be much lower than the non-lethal recordings. It should be noted that a plywood baffle was used in the non-lethal wounding protocol to dissipate the air blast from the gun to prevent the chronographs from prematurely actuating. No indication of the air blast is evident in those recordings.

Figure 6 shows a typical response for all but the closest sensors for shot locations in the abdomen, sternum and hind limb. The tissue displacement phase of the signal is present albeit very low in amplitude, but no discernable shock component of the signal is present. It is not surprising that the high frequency 'shock' components are lost over time and distance. The body's elastic and dampening nature acts to filter higher frequencies faster. Work remains to be done to characterize this phenomenon and use it to determine location of the impact.

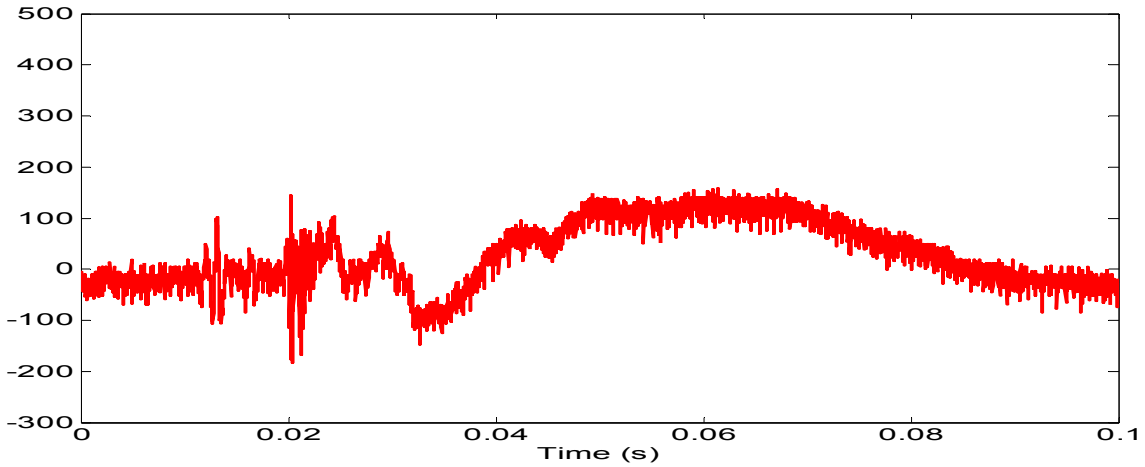

Figure 6

Signals from all sensors were digitally recorded at 50,000 samples per second on each channel with a 10, 000 Hz anti-aliasing filter. Analysis of the lateral chest shots of the pig (both amour and non-amour) revealed that the predominant shock frequencies occurred in the range of 300 to 700 Hz. Fast Fourier Transforms were performed on the shock section of each signature. The first 120 points of the shock section was zero-padded to 1024 points. The FFT returned 512 frequency coefficients over 25,000 Hz range for a resolution of 48.8 Hz per coefficient. The top two frequencies were recorded based on amplitude for each FFT. Figure 7 shows the FFT for the shock wave portion of the signal shown in Figure 5. It was quite common to see the double peaks shown in Figure 7. These peaks are considered to be harmonics.

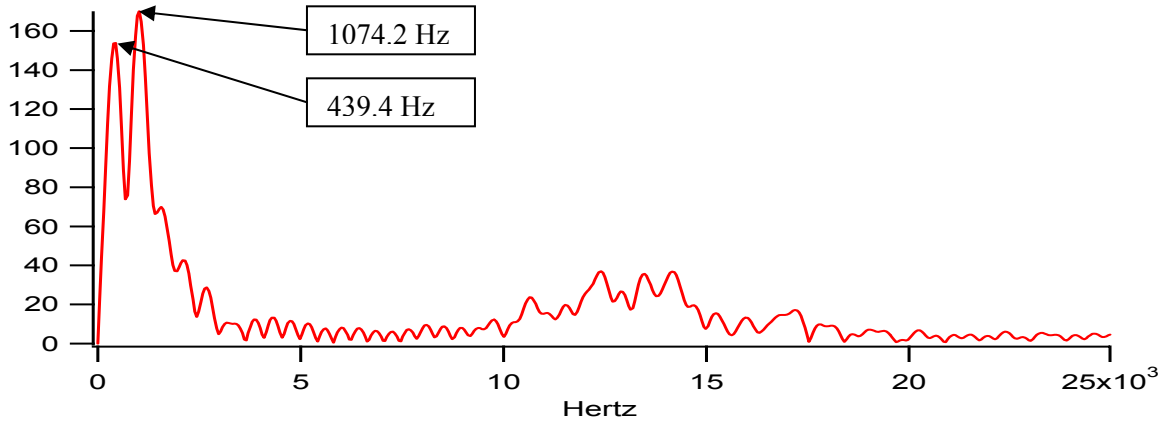

Figure 7

As stated above, while there were eight (8) sensors used on every pig for each shot, many of the recorded signatures were not of a high enough quality to perform analysis. Ninety signatures were examined for the case with body amour. These data represent signatures from sensors 1, 2, 3 and 4 for all 5 shots on all 4 pigs and sensors 5 and 6 for 5 shots each on 1 pig. Sixty (60) signatures for the unamoured case were examined. In the unamoured case, there are poor quality signals (and thus unanalyzed) on sensors 3 and 4 for pig P379 and sensor 2 for pigs P377 and P378. In the unamoured case, only P337 had 20 analyzable signatures from sensors 1 through 4. In 93% (84 of 90) of the impact signatures, one of the top two frequency peaks fell in the range between 317 to 951 Hz in the armoured cases. In the unamoured cases, 83% (50 of 60) of the signatures had one of the top two frequencies in the range of 316 – 781 Hz. Table 2 shows the averages for each pig at each sensor for the five shots at the lateral chest location while wearing body amour. In the cases where there was no top frequency in the 300 – 1000 Hz range, the most significant peak in that range was selected and the amplitude noted.

Pig ID	P337		P377		P378		P379		Totals	
	Freq-uency	Amp-litude	Freq-uency	Amp-litude	Freq-uency	Amp-litude	Freq-uency	Amp-litude	Average Frequency	Average Amplitude
Sensor 1										
Avg	434.26	141.50	454.02	4.70	600.48	272.13	400.08	254.96	472.21	168.32
SD	47.10	34.12	139.89	1.38	47.69	12.58	47.70	31.39	108.21	111.95
Sensor 2										
Avg	649.28	75.10	512.62	89.04	419.76	531.20	458.64	236.97	510.08	233.08
SD	180.79	5.42	48.70	12.54	20.51	22.36	60.76	17.56	127.24	188.76
Sensor 3										
Avg	429.32	126.24	497.88	151.94	473.38	259.58	331.88	163.10	433.12	175.22
SD	47.48	26.64	264.22	35.99	95.37	43.07	13.58	37.38	146.14	61.58
Sensor 4										
Avg	458.64	6.09	419.58	23.52	590.56	15.99	493.10	50.43	490.47	24.01
SD	95.31	2.08	43.84	7.42	179.16	3.18	55.52	3.34	118.11	17.38
Sensor 5										
Avg			385.64	44.08						
SD			36.25	21.90						
Sensor 6										
Avg			522.22	175.26						
SD			27.75	60.16						

Table 2

The location of all lateral chest shots was on the right side on the animal approximately equal distance from sensors 1 and 3. While the frequencies are tightly grouped, the amplitude for the sensor 2 shots seems too high. This sensor is on the far side of the animal and logically should be lower in amplitude then sensors 1 and 3. The amplitudes across the pigs vary greatly for sensor 2: P337 and P377 are under 100, while P378 and P379 are over 200. Removing what seems to be an outlier, P378 with amplitude of 531.20 from the average yields a revised amplitude average of 133.7 (St Dev 76.7). Similarly, sensor 1 for P377 has what seems to be

abnormally low amplitude given the fact that it is closest to the shot. Removing these shots from the overall average yields a revised sensor 1 average of 222.9 (St Dev 65.3). The coupling of the sensor to the body surface remains the largest variable to overcome. The snug fit of the body amour stabilizes the sensors and their response. The data from the armoured pigs are more consistent than the unamoured data. However, there seems to be too little coupling in the case of P377 sensor 1 resulting in low amplitude and too much coupling in P378 sensor 2 resulting in high amplitude. The data does show consistency between shots at each sensor location. This consistency is evident in the abnormally coupled shots as well. One question prior to this study concerned the response of the tissue over the course of five shots in the same location. There is no significant deviation in frequency or amplitude over the five shots.

The four animals were sacrificed and kept frozen at -20 ºC for a month at which time they were thawed and impacted again. The freeze/thaw cycle was meant to emulate the circumstances that a fresh frozen human cadaver would undergo. After thawing, the animals were impacted using the same format described above. Table 3 shows the results of the lateral chest shots with body amour, comparable to the live animal impacts summarized in Table 2. Immediately noticeable in the cadaver impacts was the lack of analyzable signatures in channels 2 and 4 in some of the animals. Theses are the sensors on the far side (non-shot side) of the pig. This loss of signal occurred in pig 379 (channel 2) and pig 337 (channel 4) with body amour, but was more prevalent on the non-body amour shots (not shown). Of those eight signatures (4 pigs channel 2 and channel 4), only pig 377 channel 2 was of sufficient signal strength and quality to analyze. Overall the top frequencies are very comparable to those of the live impacts. While the frequencies are remarkably similar, the amplitude of the cadaver signals is dramatically lower across all four sensors. Signal strength in the live animals ranged from 160 to 230 (except for sensor 4), signals in the cadavers were markedly lower: the closest sensor registering an average of 65 and sensors 2 and 3 registering 26 and 24 respectively. Sensor 4 is again understandably lower than the other sensors as it is the farthest from the shot in both scenarios.

Pig ID	P337		P377		P378		P379		Totals	
	Freq-uency	Amp-litude	Freq-uency	Amp-litude	Freq-uency	Amp-litude	Freq-uency	Amp-litude	Average Frequency	Average Amplitude
Sensor 1										
Avg	390.46	63.14	527.0	71.7	429.7	94.2	424.6	31.7	442.9	65.2
SD	71.0	24.0	47.7	4.9	21.9	8.4	50.7	11.0	70.0	26.4
Sensor 2										
Avg	468.4	51.6	615.1	9.1	473.4	17.0			519.0	25.9
SD	85.2	35.4	86.9	2.3	27.8	4.1			97.0	27.0
Sensor 3										
Avg	541.8	2.0	444.3	42.8	400.2	10.0	624.7	42.1	502.7	24.3
SD	263.6	0.8	10.7	22.4	50.6	7.5	58.9	29.9	154.6	25.8
Sensor 4										
Avg			546.7	4.0	395.3	3.1	748.4	3.5	535.0	3.5
SD			27.9	0.2	52.9	0.9	13.9	0.2	144.2	0.7

Table 3

The averages for sensors 2 and 3 are very similar that is counterintuitive since sensor 3 is much closer to the impact. This discrepancy can be accounted for since the unanalyzed signal from Pig 379 sensor 4 was not included in the average coupled with the unusually low signal recorded on sensor 3 in Pig 337. This test shows that while the key frequency components are still discernable, allowances for lower amplitudes must be made in the frozen/thawed cadaveric tissue.

Three human test subjects volunteered for the paintball impact testing. Each subject received eight impacts, four with body amour and four without body amour. Subjects received impacts in the abdomen, lateral chest with and without the amour and received two extremity shots (one arm and one thigh) wearing amour and then two more extremity shots (opposite arm and opposite thigh) while not wearing the amour. Sensors were placed on the back of the subjects and fixed with adhesive tape similar to the pigs as shown in Figure 8. Subjects wore jacket-style NATO body amour for this test. In general more of the human impact locations could be analyzed. With the exception of the sensors farthest from the extremity impacts (e.g. sensors 1 and 2 for the leg impacts), FFT data from all eight, impact locations were computed.

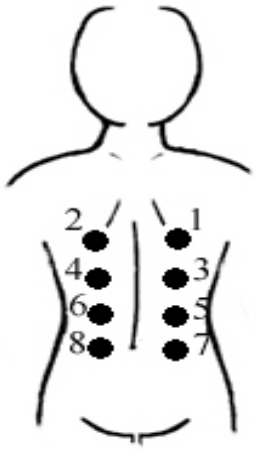

Figure 8

Figure 9 shows a representative left lateral chest impact with body amour signal from sensor 2. It should be noted that the small pre-impact waves that were visible on the swine recordings are not visible in the human recordings. As previously stated, these small waves are believed to be artefact from the air blast of the gun. Since the human subjects stand behind protective plywood it seems logical that the air blast is dissipated.

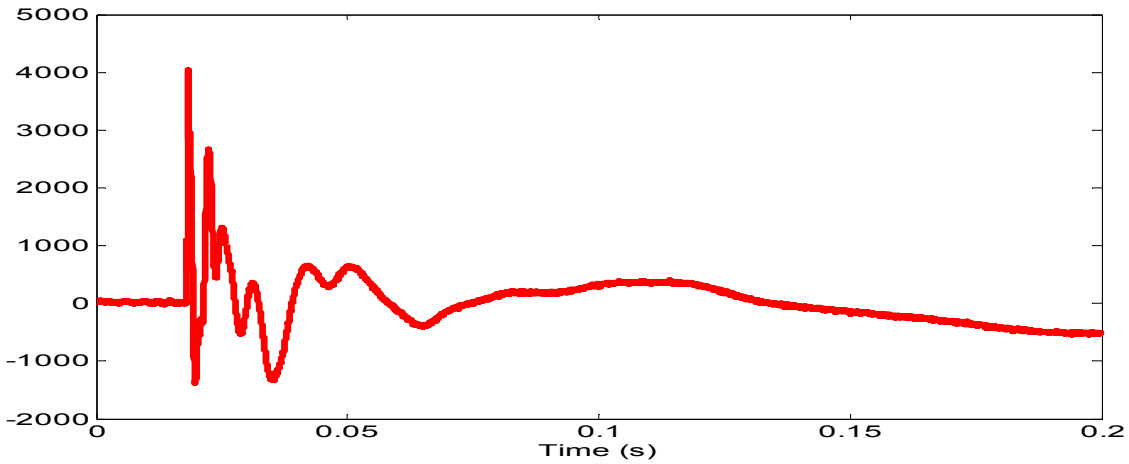

Figure 9

The human impact signature in Figure 9 seems to have shock and tissue deformation components corresponding to the swine recordings. Figure 10 shows the FFT performed on the impact shown in Figure 9. FFT analysis on the shock portion of the recordings similar to those performed on the swine impact recordings for the lateral chest impacts are summarized in Table 4.

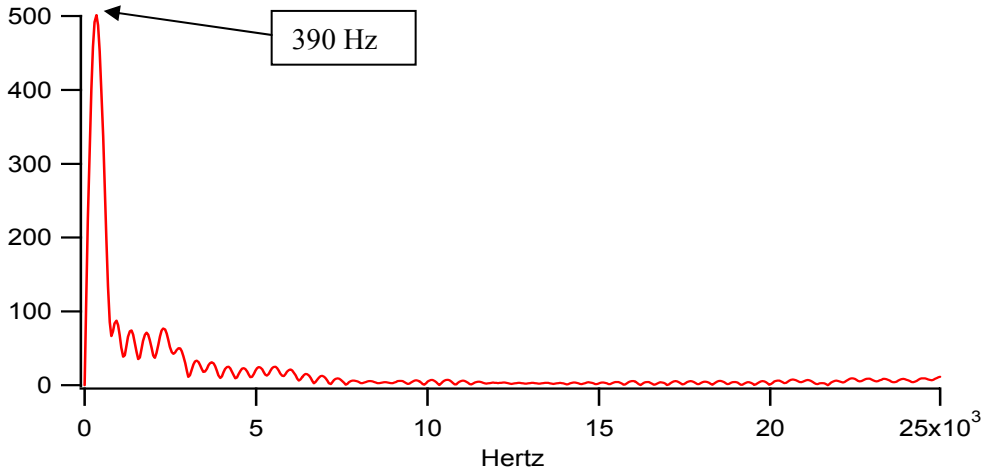

Figure 10

	Subject 1		Subject 2		Subject 3		Average	
Sensor	Frequency	Amplitude	Frequency	Amplitude	Frequency	Amplitude	Frequency	Amplitude
1	341.8	3.6	537.1	6.3	341.8	7	406.90	5.63
2	390.6	501.5	488.3	323.3	-	-	439.45	412.40
3	390.6	22.2	488.3	60.9	609.9	12.1	496.27	31.73
4	439.4	70.5	512.3	273.7	-	-	475.85	172.10
5	439.5	29.2	365.8	114.2	365.8	12.2	390.37	51.87
6	365.8	57.5	585.9	321.4	488.3	11.6	480.00	130.17
7	488.3	173.7	414.6	163.9	341.8	40.2	414.90	125.93
8	439.4	215.4	390.6	259.7	390.6	10.5	406.87	161.87

Table 4

The frequencies noted in Table 4 are all (100%) one of the top two frequency peaks in the FFTs. The lateral chest impacts for Subjects 1 and 2 occurred on the left side, therefore the even numbered sensors (2, 4, 6, and 8) are closest to the impact. This is clearly evident by the amplitudes of the peaks for subject 2; however, not as clearly the case for subject 1 as sensors 4 and 6 have lower amplitudes then what might be expected. In both cases the amplitude for sensor 1 seems lower than expected. The lower amplitudes have caused speculation that the upper two sensors, located directly below the scapulae, are not coupling as well due a shielding effect of the scapula. The protruding scapula may be preventing close contact of the vest and the sensor unit. The impact to Subject 3 was on the right side meaning that the odd-numbered sensors were closest to the impact. Subject 3 has very low amplitudes on the whole indicating either poor coupling between the sensors and the body or better protection from the body armour. In fact, the signals from sensor 2 and 4 were so weak they were not analyzed. Overall to this point, the peak frequencies of the human subject correlate well with the swine frequencies. The average frequency for the human lateral chest shots with body armour is 437.1 Hz with a standard deviation of 78.6 (n=22). The average frequency for the swine lateral chest shots with body armour is 471.1 Hz with a standard deviation of 122.0 (n=90).

2.2 High velocity impact models:

Similarities between the low impact swine and low impact human signatures provided the needed impetus to perform high velocity swine impacts. A protocol was written to perform a limited number of shots using two calibre bullets (7.62 M80 ball and 5.56 M855 ball), four locations (sternum, lateral chest, abdomen and hind limb) and three velocities (2800 ft/sec, 2300 ft/sec and 1300 ft/sec). The impact schedule is shown in Table 5. It was important to test a combination of threats facing the soldier today. Given that resources were limited, certain tradeoffs were made. The velocities were chosen to reflect an AK47 muzzle velocity (2800 ft/sec), an approximate 200-yard rifle engagement (2300 ft/sec) and handgun velocity (1300 ft/sec). 7.62-calibre rounds are currently the most common small arms threat to US soldiers on the battlefield and are fired by various Soviet Block style weapons (e.g. AK-47, RPK, RPD, etc.) The M855 round (5.56 mm) is a standard NATO round and represents the trend of reducing the bullet calibre and total round weight to gain higher velocity and decrease soldier basic ammunition load weight. This smaller calibre provides information about smaller high-velocity fragmentation munitions impacts (e.g. howitzers, mortars, grenades, etc). The chosen locations reflect the desire to maintain consistency with the low velocity protocols. However in this study, body armour was used for all impacts. The targeted population for the BIDS is the frontline combat soldier. Projected warfighter designs call for body armour. It was important in the low velocity impact study to relate back to the proof-of-concept work originally done without body amour. Therefore low impact tests were conducted wearing body amour and without body amour. The high impact tests do not need to relate back to previous low impact tests since results from these high impact tests alone will be the basis for the BIDS circuitry. Interceptor body amour from Point Blank with SAPI and Gamma Plus ceramic plates were used for this study. Sternum shots were fired into the ceramic plates of the vest, abdomen shots were fired into the Kevlar outer tactical vest just below the ceramic plates, lateral chest shots were fired into the Kevlar outer tactical vest and hind limb shots were fired into the unprotected thigh of the animal. The ceramic plates, which are rated to protect against 7.62 rounds at 2800 ft/sec, defeated all rounds at all velocities, although permanent backface deformations of approximately 1 cm were created at the high velocities. The Kevlar outer tactical vest is rated to defeat handgun rounds; however, the high ogive of the rifle rounds allowed all rounds to penetrate the Kevlar. A pilot study was performed to determine if freshly euthanized animals could be used instead of live anesthetized animals. Lateral chest shots using 7.62 rounds at 2800 ft/sec from six live anesthetized animals were compared to animals that were euthanized minutes before the impact. As in previous experiments eight sensors were placed equidistant about the spine in two columns of four. Unlike other experiments, these tests employed six newly design piezofilm sensors as well as two of the older style bone conducting sensors. Unfortunately, the new sensors were not as responsive as the older bone conducting ones and have been left out of the analysis. The results from these tests will be from signatures recorded from the two bone conducting sensors. Figure 11 shows typical impact signatures from the pilot study. The graph on the left is a 2800 ft/sec, 7.62 round, left lateral chest impact from a live, anesthetized animal. The graph on the right is the same parameter from a freshly euthanized animal.

Shot ID.	Location	Round	Amour	Velocity	Shot ID.	Location	Round	Amour	Velocity
PHV-1	Lat Chest	M80 Ball	Soft Amour	High	PHV-41	Lat Chest	M80 Ball	Soft Amour	Low
PHV-2	Lat Chest	M80 Ball	Soft Amour	High	PHV-42	Lat Chest	M80 Ball	Soft Amour	Low
PHV-3	Lat Chest	M80 Ball	Soft Amour	High	PHV-43	Lat Chest	M80 Ball	Soft Amour	Low
PHV-4	Lat Chest	M80 Ball	Soft Amour	High	PHV-44	Lat Chest	M80 Ball	Soft Amour	Low
PHV-5	Lat Chest	M80 Ball	Soft Amour	High	PHV-45	Lat Chest	M80 Ball	Soft Amour	Low
PHV-6	Sternum	M80 Ball	Plate	High	PHV-46	Sternum	M80 Ball	Plate	Low
PHV-7	Sternum	M80 Ball	Plate	High	PHV-47	Sternum	M80 Ball	Plate	Low
PHV-8	Sternum	M80 Ball	Plate	High	PHV-48	Sternum	M80 Ball	Plate	Low
PHV-9	Sternum	M80 Ball	Plate	High	PHV-49	Sternum	M80 Ball	Plate	Low
PHV-10	Sternum	M80 Ball	Plate	High	PHV-50	Sternum	M80 Ball	Plate	Low
PHV-11	Abdomen	M80 Ball	Soft Amour	High	PHV-51	Abdomen	M80 Ball	Soft Amour	Low
PHV-12	Abdomen	M80 Ball	Soft Amour	High	PHV-52	Abdomen	M80 Ball	Soft Amour	Low
PHV-13	Abdomen	M80 Ball	Soft Amour	High	PHV-53	Abdomen	M80 Ball	Soft Amour	Low
PHV-14	Abdomen	M80 Ball	Soft Amour	High	PHV-54	Abdomen	M80 Ball	Soft Amour	Low
PHV-15	Abdomen	M80 Ball	Soft Amour	High	PHV-55	Abdomen	M80 Ball	Soft Amour	Low
PHV-16	Limb	M80 Ball	No Amour	High	PHV-56	Limb	M80 Ball	No Amour	Low
PHV-17	Limb	M80 Ball	No Amour	High	PHV-57	Limb	M80 Ball	No Amour	Low
PHV-18	Limb	M80 Ball	No Amour	High	PHV-58	Limb	M80 Ball	No Amour	Low
PHV-19	Limb	M80 Ball	No Amour	High	PHV-59	Limb	M80 Ball	No Amour	Low
PHV-20	Limb	M80 Ball	No Amour	High	PHV-60	Limb	M80 Ball	No Amour	Low
PHV-21	Lat Chest	M80 Ball	Soft Amour	Medium	PHV-61	Lat Chest	M855	Soft Amour	Medium
PHV-22	Lat Chest	M80 Ball	Soft Amour	Medium	PHV-62	Lat Chest	M855	Soft Amour	Medium
PHV-23	Lat Chest	M80 Ball	Soft Amour	Medium	PHV-63	Lat Chest	M855	Soft Amour	Medium
PHV-24	Lat Chest	M80 Ball	Soft Amour	Medium	PHV-64	Lat Chest	M855	Soft Amour	Medium
PHV-25	Lat Chest	M80 Ball	Soft Amour	Medium	PHV-65	Lat Chest	M855	Soft Amour	Medium
PHV-26	Sternum	M80 Ball	Plate	Medium	PHV-66	Limb	M855	No Amour	Medium
PHV-27	Sternum	M80 Ball	Plate	Medium	PHV-67	Limb	M855	No Amour	Medium
PHV-28	Sternum	M80 Ball	Plate	Medium	PHV-68	Limb	M855	No Amour	Medium
PHV-29	Sternum	M80 Ball	Plate	Medium	PHV-69	Limb	M855	No Amour	Medium
PHV-30	Sternum	M80 Ball	Plate	Medium	PHV-70	Limb	M855	No Amour	Medium
PHV-31	Abdomen	M80 Ball	Soft Amour	Medium	PHV-71	Lat Chest	M855	Soft Amour	Low
PHV-32	Abdomen	M80 Ball	Soft Amour	Medium	PHV-72	Lat Chest	M855	Soft Amour	Low
PHV-33	Abdomen	M80 Ball	Soft Amour	Medium	PHV-73	Lat Chest	M855	Soft Amour	Low
PHV-34	Abdomen	M80 Ball	Soft Amour	Medium	PHV-74	Lat Chest	M855	Soft Amour	Low
PHV-35	Abdomen	M80 Ball	Soft Amour	Medium	PHV-75	Lat Chest	M855	Soft Amour	Low
PHV-36	Limb	M80 Ball	No Amour	Medium	PHV-76	Limb	M855	No Amour	Low
PHV-37	Limb	M80 Ball	No Amour	Medium	PHV-77	Limb	M855	No Amour	Low
PHV-38	Limb	M80 Ball	No Amour	Medium	PHV-78	Limb	M855	No Amour	Low
PHV-39	Limb	M80 Ball	No Amour	Medium	PHV-79	Limb	M855	No Amour	Low
PHV-40	Limb	M80 Ball	No Amour	Medium	PHV-80	Limb	M855	No Amour	Low

Table 5

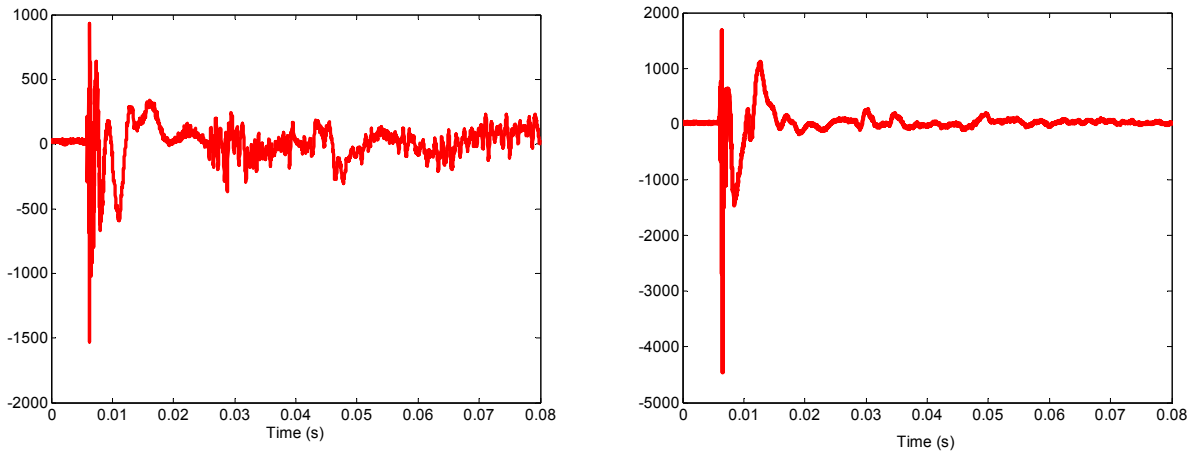

Figure 11

Similarly Figure 12 shows the frequency spectrum of the above impact signatures: live on the left and freshly euthanized on the right. The FFTs below are 1024 point FFTs using 75 data points (1.5 ms) and zero-padding. The y-axis is always in arbitrary units which can be compared between graphs in which similar processing has been performed. After completing the pilot study, the remaining animals were impacted directly after euthanasia. It should be noted that the sensor used in these recordings has a particular resonance at 17,000 Hz explaining the large frequency response in that area on the graphs in Figure 12. While there was some signal present in that frequency region, care must be used in characterizing the frequency response of the sensors as it affects the analysis of the impact signatures.

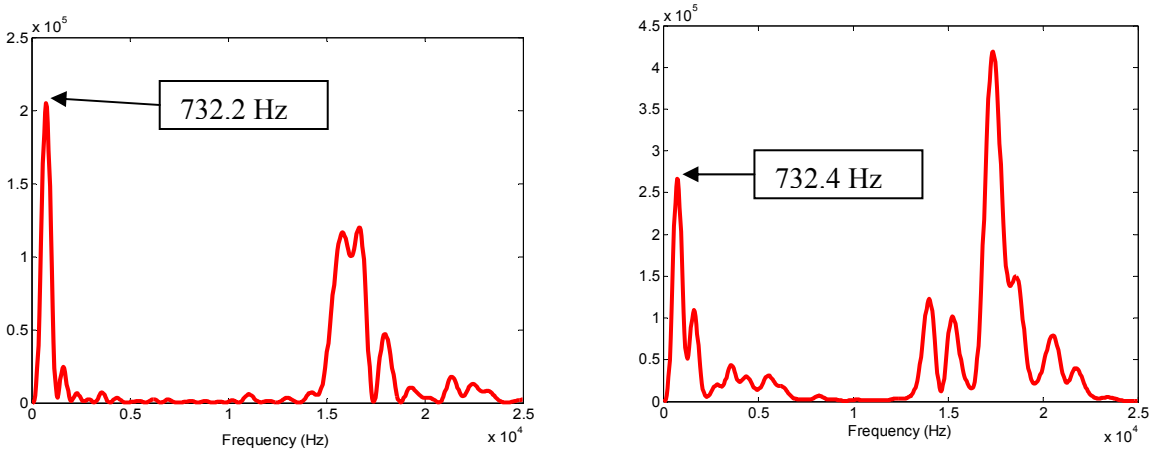

Figure 12

Forty pigs ranging in weight from 41.8 – 74.9 kg have been used in the testing to date. In an effort to conserve animals, most animals were shot twice. Shots to the hind limb and lateral chest were executed serially (hind limb first) while the pig was in a recumbent position. Similarly, abdomen and sternum shots were executed will the animal was suspended in an upright position. Because the shot distal to the sensors was carried out

first, it is assumed from visual inspection that damage to the animal was not sufficient enough to negatively impact second shot signature.

Location	Calibre	Velocity (ft/sec)	Ch 5 Freq	Ch 5 Amp	Average Freq	Average Amp	Ch 6 Freq	Ch 6 Amp	Average Freq	Average Amp
Abdomen	7.62	2825	659.18	1.02E+07			390.63	5.95E+07		
Abdomen	7.62	2817	463.87	3.78E+06	500.49	1.16E+07	610.35	3.00E+07	610.35	3.00E+07
Abdomen	7.62	2800	463.87	2.13E+07	108.27	7.23E+06	415.04	8.02E+06	98.67	2.27E+07
Abdomen	7.62	2782	415.04	1.10E+07			488.28	4.91E+07		
Abdomen	7.62	2371	488.28	6.04E+06			366.21	2.81E+07		
Abdomen	7.62	2307	585.94	1.20E+07	500.49	2.02E+07	488.28	2.52E+07	500.49	1.59E+07
Abdomen	7.62	2306	366.21	3.76E+07	98.67	1.41E+07	439.45	2.13E+06	147.16	1.28E+07
Abdomen	7.62	2300	561.52	2.52E+07			708.01	8.00E+06		
Abdomen	7.62	1328	366.21	1.13E+07			366.21	3.42E+07		
Abdomen	7.62	1316	366.21	1.91E+07	423.18	1.14E+07	488.28	1.95E+07	406.90	1.83E+07
Abdomen	7.62	1295	537.11	3.77E+06	98.67	7.69E+06	366.21	1.28E+06	70.48	1.65E+07
Hind	7.62	2802	659.18	4.89E+04			366.21	1.52E+05		
Hind	7.62	2800	463.87	6.75E+04			439.45	6.61E+05		
Hind	7.62	2789	366.21	1.30E+04			439.45	4.39E+05		
Hind	7.62	2787	463.87	1.31E+05	454.10	4.96E+04	488.28	2.36E+06	434.57	2.70E+06
Hind	7.62	2781	488.28	2.54E+04	50.63	5.08E+04	366.21	1.05E+06	43.67	3.59E+06
Hind	7.62	2773	488.28	1.13E+04			439.45	8.99E+06		
Hind	7.62	2334	366.21	5.87E+04			366.21	7.28E+05		
Hind	7.62	2321	366.21	3.90E+04			390.63	1.16E+07		
Hind	7.62	2300	439.45	4.65E+04	380.86	6.61E+04	366.21	3.60E+05	444.34	3.36E+06
Hind	7.62	2285	366.21	1.71E+05	32.75	6.04E+04	415.04	3.79E+06	135.27	4.83E+06
Hind	7.62	2281	366.21	1.59E+04			683.59	3.05E+05		
Hind	7.62	1330	366.21	2.62E+04			390.63	1.24E+04		
Hind	7.62	1320	585.94	1.02E+04			439.45	3.04E+04		
Hind	7.62	1317	488.28	6.01E+03	454.10	1.05E+04	366.21	1.14E+04	434.57	3.38E+04
Hind	7.62	1289	366.21	3.02E+03	92.32	9.15E+03	610.35	4.43E+04	102.71	2.46E+04
Hind	7.62	1270	463.87	6.95E+03			366.21	7.04E+04		
Hind	5.56	2380	781.25	3.20E+03			390.63	542.4916		
Hind	5.56	2342	561.52	2.42E+04	518.80	1.08E+04	463.87	1.06E+04	408.94	1.22E+04
Hind	5.56	2339	366.21	2.84E+03	197.71	1.01E+04	415.04	8.11E+03	41.69	1.23E+04
Hind	5.56	2290	366.21	1.32E+04			366.21	2.95E+04		
Hind	5.56	1450	463.87	271.23			463.87	9.06E+03		
Hind	5.56	1349	512.70	1.98E+03	488.28	2.87E+03	415.04	3.35E+03	421.14	4.08E+03
Hind	5.56	1307	488.28	7.12E+03	19.93	2.95E+03	439.45	3.31E+03	406.90	3.31E+03
Hind	5.56	1213	488.28	2.10E+03			366.21	609.6323		

Lat Chest	7.62	2800	390.63	1.37E+06			805.66	8.57E+07		
Lat Chest	7.62	2800	366.21	1.08E+06	382.49	9.75E+05	366.21	1.57E+08	512.70	9.83E+07
Lat Chest	7.62	2788	390.63	4.72E+05	14.10	4.60E+05	366.21	5.24E+07	253.72	5.33E+07
Lat Chest	7.62	2777	390.63	3.43E+06			561.52	1.34E+08		
Lat Chest	7.62	2748	366.21	3.14E+06	455.73	2.93E+06	659.18	2.70E+07	528.97	6.37E+07
Lat Chest	7.62	2742	610.35	2.23E+06	134.46	6.29E+05	366.21	3.03E+07	149.17	6.07E+07
Lat Chest	7.62	2378	537.11	1.48E+05			439.45	7.31E+06		
Lat Chest	7.62	2341	415.04	7.35E+05			439.45	3.18E+06		
Lat Chest	7.62	2292	366.21	1.09E+07	439.45	2.87E+06	366.21	2.68E+08	444.34	8.93E+07
Lat Chest	7.62	2290	366.21	2.25E+06	80.97	4.55E+06	366.21	1.31E+08	99.77	1.12E+08
Lat Chest	7.62	2261	512.70	3.26E+05			610.35	3.71E+07		
Lat Chest	7.62	1325	415.04	4.52E+06			439.45	1.88E+06		
Lat Chest	7.62	1320	463.87	1.16E+05			390.63	3.12E+07		
Lat Chest	7.62	1320	463.87	4.81E+05	488.28	2.11E+06	366.21	2.04E+07	458.98	1.22E+07
Lat Chest	7.62	1284	634.77	1.45E+06	84.57	2.02E+06	537.11	3.98E+06	87.00	1.30E+07
Lat Chest	7.62	1275	463.87	3.98E+06			561.52	3.71E+06		
Lat Chest	5.56	2372	390.63	4.54E+06			366.21	1.63E+08		
Lat Chest	5.56	2356	366.21	9.18E+05	402.83	4.40E+06	463.87	2.28E+06	433.35	4.17E+07
Lat Chest	5.56	2341	366.21	2.39E+05	58.12	5.35E+06	512.70	8.45E+04	67.23	8.10E+07
Lat Chest	5.56	2305	488.28	1.19E+07			390.63	1.33E+06		
Lat Chest	5.56	1408	366.21	1.77E+06			659.18	5.96E+04		
Lat Chest	5.56	1393	366.21	4.20E+05	402.83	4.36E+06	366.21	1.75E+05	451.66	1.30E+05
Lat Chest	5.56	1313	512.70	1.26E+07	73.24	5.59E+06	415.04	2.73E+05	140.25	1.17E+05
Lat Chest	5.56	1309	366.21	2.62E+06			366.21	1.16E+04		
Sternum	7.62	2832	366.21	1.25E+05			463.87	7.78E+04		
Sternum	7.62	2774	366.21	1.05E+05			366.21	1.82E+04		
Sternum	7.62	2760	561.52	1.80E+04	447.59	1.49E+05	488.28	2.62E+04	406.90	5.76E+04
Sternum	7.62	2409	415.04	3.23E+05	101.64	1.57E+05	366.21	1.28E+05	70.48	6.14E+04
Sternum	7.62	2364	366.21	2.74E+05			366.21	3.36E+05		
Sternum	7.62	2306	390.63	1.99E+05	390.63	1.58E+05	439.45	8.98E+04	390.62	1.74E+05
Sternum	7.62	2209	415.04	397.3958	24.41	141523.83	366.21	9.64E+04	42.29	1.40E+05
Sternum	7.62	1363	366.21	6.06E+03			366.21	1.69E+03		
Sternum	7.62	1313	366.21	6.63E+04	415.04	2.59E+04	439.45	5.48E+04	482.18	3.20E+04
Sternum	7.62	1300	561.52	6.35E+03	97.66	2.83E+04	439.45	1.36E+03	138.65	3.57E+04

Table 6

Table 6 shows the frequency component analysis of the high velocity impacts on the swine. The table shows the FFT analysis of the first 7.5 ms of the shock wave. While eight sensors were affixed to the animal, this

table represents the signals from two sensors, channels 5 and 6. For impacts to the lateral chest and the hind limb, channel 5 was closest to the entry wound and channel 6 was closest to the exit wound. For sternum shots and abdomen shots the sensors were equidistant from impacts. As previously mentioned there was no penetration of the ceramic ballistic plates for sternum shots. There were exit wounds for all other shots except some of the 5.56 calibre shots at 1300 ft/sec. In the analysis in Table 6, the frequency between 350 Hz and 1000 Hz with the highest power was recorded in this table. In many cases this was not the highest powered frequency in the spectrum. For channel 5, in 53 of the 69 shots, the peak in this 350-1000 Hz range was not the frequency of largest power. In 8 of the 53 cases the largest frequency peak was higher than 1000 Hz and in the rest of the cases the highest power was below 350 Hz. For channel 6, roughly half of the highest powered frequencies fell into the 350-1000 Hz range (33 out of 69). This discrepancy seems to be due to the shape of the bullet (i.e. the ogive). The high ogive of the rounds, necessary for stability during supersonic flight, penetrates the skin without causing the impact expected for a projectile of such weight and velocity. The spherical shapes used in the proof-of-concept less than lethal tests produced a more distinct shock frequency that in every case produced the highest powered frequency in the 500-1000 Hz range. With rifle bullets, the shock wave epoch is much shorter, on the order of 3 ms. Therefore FFT analysis over 7.5 ms tends to include more of the lower frequency tissue displacement segment resulting in high powered lower frequencies. Also of note is the discrepancy in power between channel 5 and channel 6 in the lateral chest shots. In almost all cases, the channel 6 frequencies are markedly (at least 10 times) higher than their counterparts from channel 5. Only in the 5.56- calibre shots at 1300 ft/sec does this tendency reverse. Almost everyone is familiar with the size difference between the entry and exit wounds from a gunshot. There was no exception to that understanding in these tests. As the bullet passes through the body it tumbles creating a large exit wound. While the entry wound was rarely much larger than the calibre, the exit wound was normally 4+ cm in diameter. This is presumably the cause of the higher powers noticed on the exit side (channel 6). In the cases of the low velocity 5.56 round impacts on the lateral chest there are no exit wounds resulting in a much lower power than the entry side.

2.3 Blast Overpressure Impacts

In July 2002, testing was conducted under an approved human use protocol at the Aberdeen Test Center (ATC) to assess the effectiveness of blast suits against anti-personnel mines. This was a multi-agency/service effort involving ATC, the Medical Research and Materiel Command, the University of Virginia, the Walter Reed Army Medical Center, the Uniformed Services University of the Health Sciences, and the Armed Forces Institute of Pathology, which was funded by the Communications and Electronics Command, Humanitarian Demining effort.

Mine surrogates containing 100 and 200 g of C4 explosive were used against cadavers with and without the blast suit. Sensors were affixed to the cadavers using superglue in the same configuration as Figure 8. Signals were recorded at 50,000 samples per second on each channel. Figure 13 shows the impact signal from a 200-g blast with a blast suit. The subject's nose was 55 cm (measured radially) from the centre of the mine surrogate. The response from the sensor seems to be that of a second-order system in response to a step function. Figure 13 shows a longer duration event lasting well beyond 400 ms. Examination of the recording indicates higher frequency components for the first 150 ms and slower frequencies after 150 ms. It is likely that part of the slower frequency waves are made up of the tissue deformation waves. An FFT on the first 170 ms of the blast is shown in Figure 14. Much of the response to this type of blast is in the lower frequencies, less than 200 Hz. This seems to indicate that the surface of the body couples with the primary low frequency blast wave. However there are significant components in the frequency range (400-1000 Hz) identified in the impact tests that can be exploited by a detection system. For clarity, a partial spectrum (0-10000 Hz) is shown.

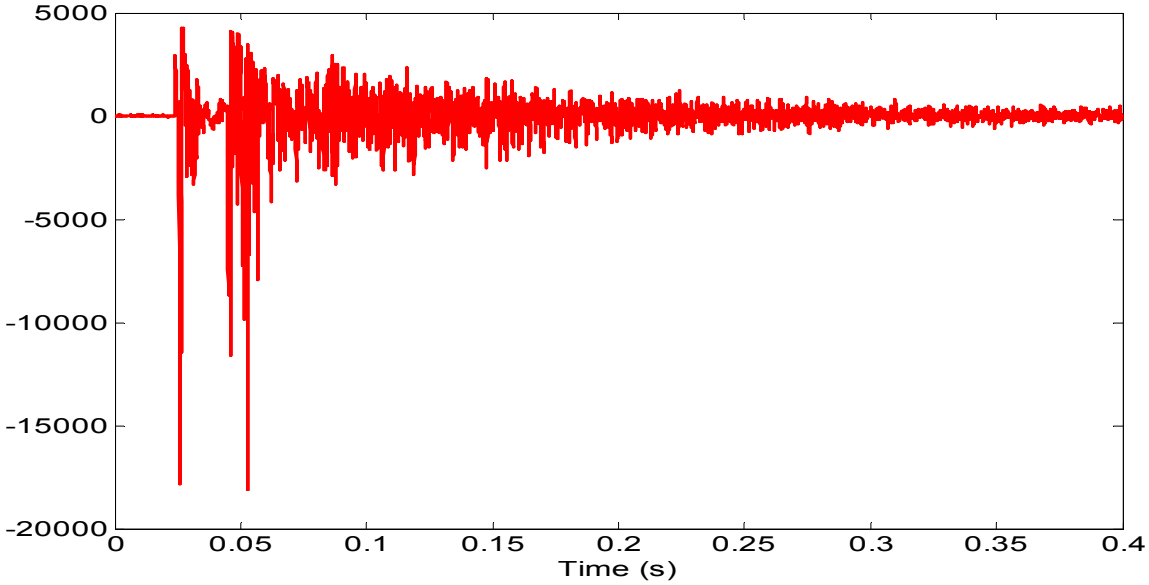

Figure 13

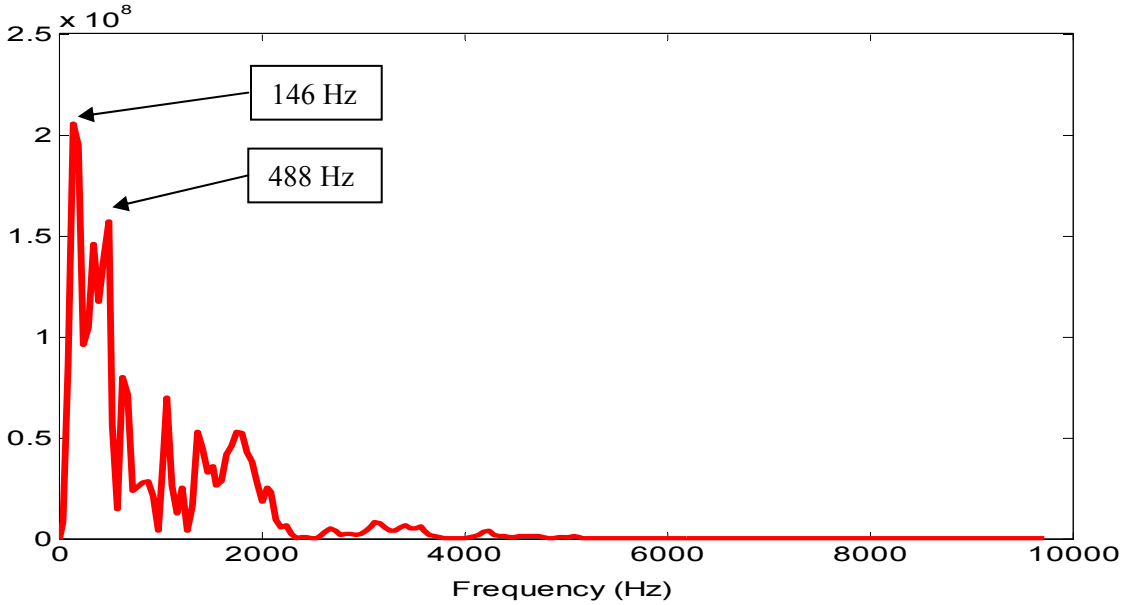

Figure 14

2.4 Normal Activity

Data was also acquired for simulated normal activity to determine key characteristics of signals from running, hopping and a significant jolt. Human data was collected while the subject ran and hopped in place. The jolt signature resulted in a jump off a 36-inch table. Figure 15 is the resultant signal from the 36-inch jump. Figure 16 is the frequency domain spectrum produced by the FFT. The frequency spectrum shows that

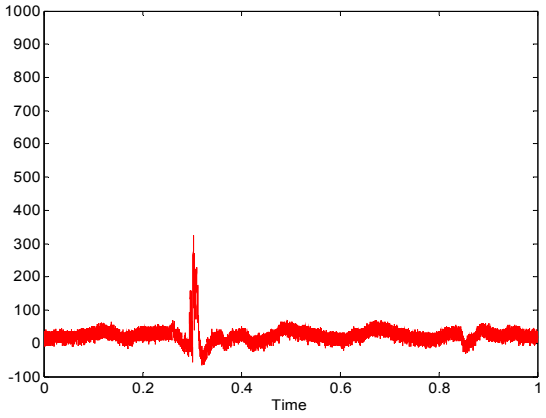

Figure 15

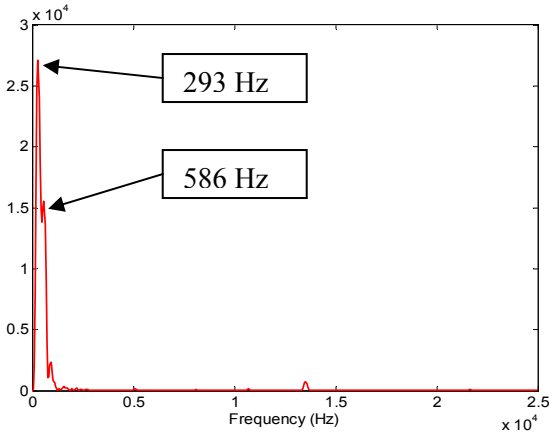

Figure 16

the jolt to the body produces two significant frequencies: a larger amplitude component at 293 Hz and a smaller but significant frequency at 586 Hz. This latter frequency is in the range produced by the bullet. Of the three 'normal' recordings, only the big jump proved to contain frequencies in the range of those produced by the bullet impacts.

3.0 BIDS DESIGN

The BIDS design requirements centred on reducing false-positive indications to near zero. It would be approaching impossibility to completely rule out false-positive indications due to the number of 'normal' tests on all body types necessary. Because the BIDS was soldier-born, they were always requirements of near-zero cube, weight and power. An analogue based system was designed based on the proof-of-concept data. Testing from the proof-of-concept phase indicated that discrimination could be achieved by isolating frequencies in the 400-1000 Hz band. If these frequencies met a threshold voltage requirement, an impact criterion would be met. While high velocity swine tests corroborated the earlier proof-of-concept tests in terms of the frequency range of interest, it was decided to employ a high-pass filter for the circuit.

The circuitry for BIDS could be purely digital in nature or an analogue-digital hybrid. In its current embodiment, the circuitry is primarily analogue with a digital output that is compatible with computing devices. The low power analogue components allow the system to be 'on', in a listening mode, continuously. To meet power requirements, a digital system would have to incorporate sophisticated wake-up circuitry which would allow the microprocessor to reside in a sleep state until a signal of interest required processing. The current embodiment is described below and shown in Figure 17. The BIDS consists of two sensors that couple to the body in such a way as to sense the vibrations in the skin. The sensors are piezo-film mounted on a flexible substrate of Mylar plastic. The vibrations produce a voltage commensurate to the frequency and amplitude of the vibrations. Each sensor signal is processed in similar circuit sections. All sensor signals are ultimately fed into logic circuitry that makes a determination as to the location of the impact. Two circuit sections are shown below, one section will be described here.

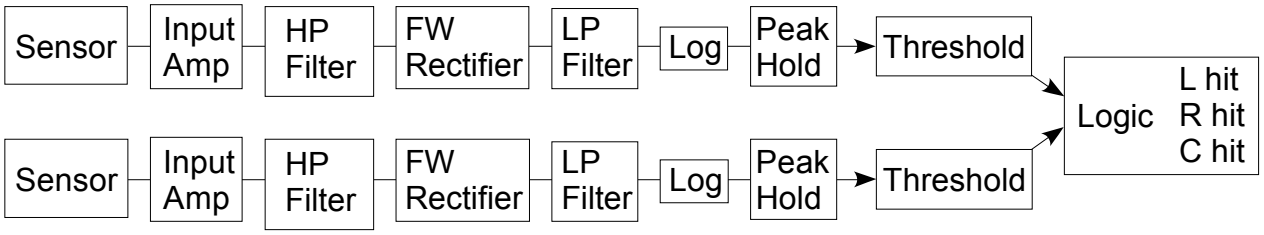

Figure 17

The voltage signal is conducted to an input buffer amplifier. The signal then passes through a high pass filter. The current embodiment uses a 3-pole Bessel with a cut-off frequency of 5000 Hz. While much of the work to date indicates that telltale frequencies exist in to 400-1000 Hz range, it is impossible to create an analogy filter with such a narrow band pass. The 5000 Hz filter is 42 dB down at 1000 Hz and 60 dB down at 500 Hz. We've found that there is enough frequency information passed by this filter to adequately discriminate the impact signals collected to date. The signal is then conducted to a full-wave rectifier which converts the voltage from bipolar to only positive. The signal then passes through a 3-pole 1000 Hz low pass filter which widens the voltage peaks of interest. The signal is then conducted into a logarithmic amplifier. The output of this amplifier stage is a voltage equal to the log of the input voltage. This stage prevents a large signal from saturating the next stages. Saturation would cause loss of frequency information that could lead to false-positive impact determinations. The next stage is a peak hold circuit which determines and conducts the peak voltage in the signal to the threshold circuit stage. The threshold section compares the peak voltage of the signal to a threshold reference voltage. If the signal voltage is higher than the threshold reference then an impact has occurred. The original signal voltage is passed to the logic that determines location. The location logic compares the amplitudes of all the sensors to make a location determination. In the current two-sensor embodiment, if the amplitude signals from the two sensors are less than a 2:1 ratio and at least one sensor signal meets the threshold voltage requirement, the impact is deemed to have occurred between the sensors, or in a centre location. If the ratio of the signals is greater than 2:1 and the greater signal also meets the threshold voltage requirement, the location is deemed to be distal to the sensor with the greater amplitude signal. Thus in the two sensor embodiment, three locations are possible: centre, right and left. The voltage signals for these location outputs are latched and then available to be read or transmitted to a computer. Once read, the BIDS accepts a reset voltage signal which returns the location outputs to ground. In its current embodiment, the BIDS circuitry can distinguish one impact in each location until a reset is received. The current analogy BIDS circuit measures 1.5 square inches and requires approximately 600 microamperes of current at 3 volts. Bench testing of the BIDS circuit consisted of converting the digital impact signatures in analogy voltages and feeding them through the circuit. The impact threshold settings were set to discriminate between the swine impacts and the normal human movement signatures. Setting the threshold is somewhat arbitrary since the voltage at that point is dependent upon the initial amplification from the input amplifier. More important is the relative voltage levels between the smallest detectable impact and the largest normal movement signal. Figure 18 shows a comparison of two signals that have been filtered using the 3-pole 5000 Hz high pass filter in the BIDS circuit. The blue trace is the time domain signal from a hind limb, 5.56 calibre impact at 1300 ft/sec; the red trace is the time domain signal from the big jump in Figure 15. Figure 18 shows the ability to easily discriminate the weakest bullet impact recorded from the strongest 'normal' activity recording.

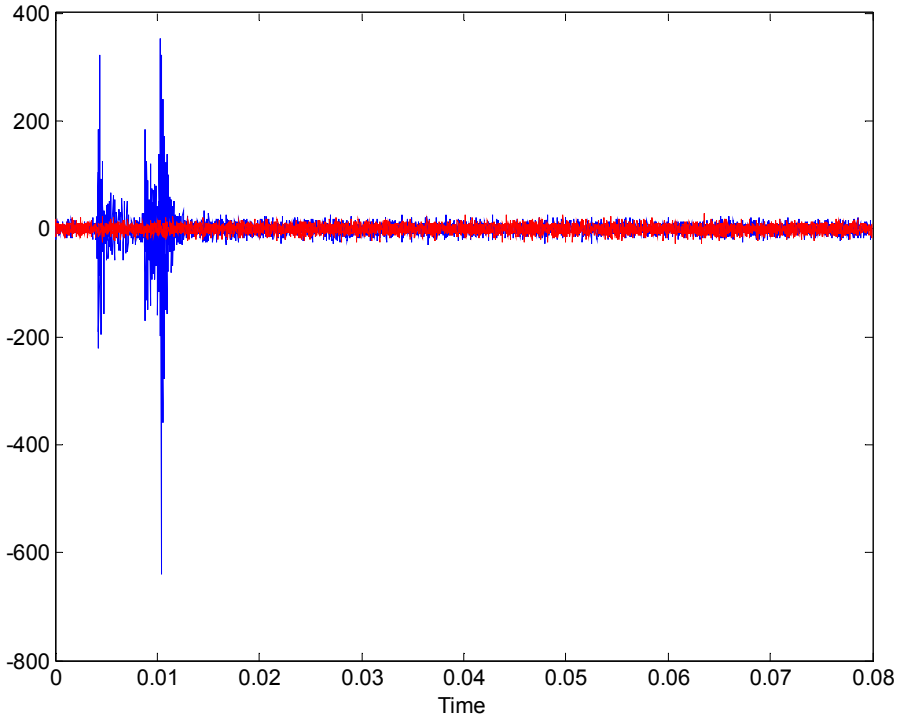

Figure 18

3.1 Future Work

The current embodiment of BIDS will be integrated into the WPSM and tested for false-positive indications during normal soldier activity. In parallel, validation testing using human surrogates will begin with the low impact paintball model validation studies. If the model is adequate, high velocity impact testing will be initiated.

A further aspect of BIDS is linking the impact detection with the wounding severity to provide the medic with as much triage information remotely as possible. Pathology reports for all the high velocity impacts conducted will be analyzed in conjunction with the impact signatures to establish a relationship between the impact signature and the resulting wound. In the future it is anticipated that the BIDS can be based on a digital signal processor which would sample the incoming analogy voltage from the sensors, perform Fast Fourier Transforms and power analysis on the signals to better determine impacts and locations. It is quite possible that sophisticated algorithms could tell from frequency analysis whether bone has been struck and from power analysis whether an exit wound exists as well as better wound localization. In this digital embodiment, BIDS could track multiple impacts in the same general location, as well as potentially providing indication of wounding severity.

4.0 REFERENCES:

[1] Army White Paper: Concepts for the Objective Force

[2] Bellamy, R. F., The causes of death in conventional land warfare: implication for combat casualty care research. Milit Med vol. 149 no. 55, 1984.

[3] Carey, Michael E. Analysis of Wounds Incurred by U.S. Army Seventh Corps Personnel Treated in Corps Hospitals during Operation Desert Storm, February 20 to March 10,1991. J of Trauma vol. 40 no. 3, 1996

Acknowledgements

The authors would like to acknowledge the following people:

Dr. Robert Matthews and Linas Kunstmanas from Quantum Applied Science and Research, San Diego, California for their insight into the circuit design.

LTC Terrell Blanchard and MAJ David Bentzel at the Armed Forces Institute of Pathology, Washington, D.C. for their invaluable assistance during the high velocity swine protocol.

M. Steven Rountree from Amtec Corporation for his assistance on the paintball protocols

Dr. C. Dale Bass and Dr. Robert Harris for allowing participation in the landmine protocol.

Research was conducted in compliance with the Animal Welfare Act and other Federal statutes and regulations related to animals and experiments involving animals and adheres to principles stated in the Guide to the Care and Use of Laboratory Animals, National Research Council.

Material has been reviewed by the Walter Reed Army Institute of Research. There is no objection to its presentation and/or publication. The views of the authors do not purport to reflect the position of the Department of the Army or the Department of Defense, (para 4-3), AR 360.5.